Health Indicator Development for Low-Voltage Battery Diagnostics and Prognostics in Electric Vehicles

Xinyu Du[1], Huaizheng Mu[2], Kevin Corr[3], Matt Nowak[4], Hong Wang[5], Tung-Wah Frederick Chang[6], and Sara Rahimifard[7]

[1,2,3,4]*General Motors Global Technical Center, Warren, Michigan, 78092, USA*

xinyu.du@gm.com
huaizheng.mu@gm.com
kevin.corr@gm.com
mateusz.nowak@gm.com

[5,6,7]*General Motors Canadian Technical Center, Markham, Ontario, L3R4H8, Canada*

hong.wong@gm.com
tung-wahfrederick.chang@gm.com
sarasadat.rahimifard@gm.com

ABSTRACT

Each electric vehicle (EV) requires a low-voltage (*e.g.*, 12V) auxiliary battery to provide electric power to onboard electronic control units, lighting systems, and various sensors during power off. Therefore, when the low-voltage battery is in low state of health (SOH) or low state of charge (SOC), it may cause no-start events. The existing OnStar Proactive Alert service can effectively predict low SOC or low SOH events for low-voltage batteries in Internal Combustion Engine vehicles using cranking signals. However, it does not work for EVs since there is no cranking event. In this work, a diagnostic and prognostic solution for the low-voltage battery of EVs is proposed. Four novel health indicators (HIs) along with the decision-making system are developed based on equivalent circuit models. Furthermore, the selection process of appropriate HIs tailored to various operational states of the vehicle is described. The validation results based on GM test EV data have demonstrated the effectiveness and robustness of the proposed solution.

1. INTRODUCTION

The move towards zero emissions has led to the fast growth of electric vehicles (EVs) as a practical alternative to traditional internal combustion engine vehicles (ICE). EVs are acclaimed for their environmental benefits and reduced operational costs. Electric vehicles commonly incorporate high-voltage (HV) batteries as their primary power source, complemented by a secondary 12V low-voltage (LV) auxiliary battery. The LV battery supplies power to various auxiliary systems such as lights, audio systems, air conditioning, electronic control units (ECUs), power windows and infotainment system (Emadi, Williamson, & A. Khaligh, 2006) (Hou, Magne, Bilgin, & Emadi, 2015) (Hasan, Mahmud, Habib, Motakabber, & Islam, 2021) (Wang, Zheng, & J. Bauman, 2023). These auxiliary systems play crucial roles in the normal operation of electric vehicles, underscoring the critical importance of the LV battery.

Although the LV battery is not responsible for directly powering the electric vehicle, its malfunction can yield significant consequences. First, the LV battery supplies electric power to the vehicle's ECUs during startup; a faulty battery may result in no-start events. Second, various low voltage electric systems rely on the 12V battery. A faulty battery may render these systems inoperative. In some situations, it may impact propulsion system, steering system, or braking system (*e.g.*, Anti-lock Braking Systems (ABS), Electronic Stability Systems (ESC)). Last but not the least, the charging system and cooling system for HV batteries rely on the 12V battery. A faulty LV battery may lead to malfunction of HV battery thermal control in some corner cases. In summary, the health of the 12V battery is critical to ensure EV performance.

For current ICE vehicles, LV battery diagnostics and prognostics rely on cranking signals (Du & Zhang, 2018), which is unavailable for EVs. Making it even more challenging is the fact that the LV battery in EV lacks excitation since the battery is under charging most of time during driving or during power off with external charger plugged in for HV batteries. To this end, the existing LV battery prognostic algorithms for ICE vehicles can't be

directly applied to EVs. Therefore, there is a need to develop a new prognostics framework with a set of battery health indicators (HIs) to assess the health state of the LV battery. The development work includes identifying enabling conditions which make HI robust and accurate, selecting a set of HIs from the plurality of HI candidates based on the prognostic capability, estimating the value of each HI, and determining whether the LV battery system is healthy or faulty based on selected HIs.

The development of HIs poses several challenges. First, the real driving condition includes multiple modes, such as power-off, power-on but not starting, and different driving modes. Different modes can lead to nonlinearity, which is difficult to be handled by a simple diagnostic method. Second, noise can be introduced from the sensors, motors, or electronic devices, which pose robustness concern for HIs. Third, internal resistance is a crucial battery performance metric, yet resistance estimation may be challenging due to insufficient excitation conditions in most scenarios and limited computational capabilities of onboard ECUs. From the vehicle driving profile shown in Figure 1, it's hard to find a line with a positive slope to calculate the battery internal resistance. Please note that the battery internal resistance can be calculated from $\frac{dV}{dI}$, when the open circuit voltage (OCV) is not changed based on the 2-parameter equivalent circuit model. Further, the temperature may influence the battery performance, thereby demanding the algorithm's stability across different temperature ranges to be considered.

In this work, we propose a novel prognostic solution for LV batteries in EVs to early detect battery failures, *i.e.*, high internal resistance fault. The proposed prognostic solution takes existing signals, voltage, current, state of charge (SOC), and temperature as the inputs. Data collection was performed on one test electric vehicle and two 12V lead-acid batteries, healthy and faulty, respectively, with a wide range of driving scenarios and temperature fluctuations. More details are described in Section 4.1. Several HIs have been developed and customized to suit various vehicle operational states. The contributions of this work can be summarized as follows:

1) We have developed and evaluated multiple health indicators specifically for LV battery diagnostics and prognostics for EVs. These HIs are based on both physical analysis and battery voltage/current data including internal resistance during charge or discharge ($RhoC$, $RhoD$), internal resistance under charge-transition or discharge-transition phase (R_c, R_d) and corresponding OCV (OCV_c, OCV_d), normalized ripple resistance (R_n), capacity deviation ($\frac{dQ}{dV}$), peak current and corresponding peak voltage ($Peak_I$, $Peak_V$).
2) The performance of each HI under various driving modes is evaluated using real vehicle test data. $RhoC$, R_d, R_n and $\frac{dQ}{dV}$ are selected as effective HIs.

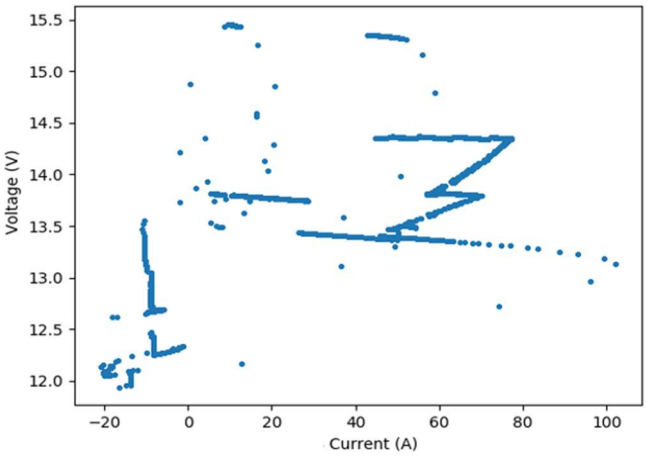

Figure 1. The curve of current vs voltage under real drive scenario.

3) We have conducted an analysis under different usage conditions to evaluate the impact of temperature variation and SOC fluctuation. This approach achieves high robustness in different conditions.
4) We have demonstrated our system functions at 10ms/sample and 200ms/sample, respectively, which indicates our system can be applied to both onboard and off-board prognostic system.

2. RELATED WORK

The existing battery prognostic methods primarily fall into two categories: data-driven approaches and physics-based/heuristic-based approaches.

Data-driven methods leverage machine learning models, input data and corresponding labels to automatically discover features and make decisions. Popular data-driven approaches include support vector machine, decision tree, gaussian process, logistic regression, or neural network (Khan & T. Yairi, 2018) (Zhao, Zhang, & Ge, 2016). For battery remaining useful life estimation, a naive Bayes model was applied in (Ng, Xing, & Tsui, 2014), and a polynomial regression model was developed in (Xing, Ma, Tsui, & Pecht, 2013). For battery fault diagnostics or prognostics, a fusion of Genetic Algorithm (GA) and Back Propagation Neural Network approach is developed in (Samanta, Chowdhuri, & Williamson, 2021), where GA was utilized to initialize and optimize the connection weights and thresholds of the neural network. In (Naha, et al., 2020), a random forest classifier was applied to detect internal short-circuit faults and achieved high accuracy. However, data-driven approaches face several challenges in practical applications. First, a large amount of data for training and validation are required to uncover meaningful features and achieve good performance (Ng, Xing, & Tsui, 2014). Second, it is difficult to implement onboard due to the computational limitations of on-board ECUs in vehicles (Cheng, Azarian, & Pecht, 2010). Third, the corner case data is rare, especially under different driving

conditions. This imbalance can lead to biased or incomplete models that may not perform well when encountering these corner cases in real-world situations.

Compared to data-driven methods, physics-based approaches involve the development of HIs based on battery models and physical analysis (Cheng, Azarian, & Pecht, 2010). Prognostics are achieved by comparing the results of these HIs. For example, the LV battery prognostic solutions developed in (Du & Zhang, 2018) are tailored to ICE vehicles. The solution relies on cranking signals. When the battery resistance increases, the crank time is prolonged, and the crank resistance ratio is increased. Physics-based approaches have several advantages. First, physics-based methods do not require large amounts of data since prognostics are developed based on knowledge. Second is the ease of implementation. Some physics-based/heuristic-based methods are easy to apply in practical products due to the relatively simple structure (*e.g.*, equivalent circuit model). The model tuning is also relatively easy and straightforward due to its clear physical interpretations. Please note some physics-based approaches are complicated and are more suitable for offboard validation, *e.g.*, the finite element model or electrochemical models. Third, the explainability is much better for physics-based approaches than data-driven approaches, offering great traceability for debugging and refinement in the event of a spill of false positive detections.

For electric vehicles, the cranking signals including cranking time or cranking resistance are not available, which poses a significant challenge when adopting the existing LV battery prognostics algorithms. Other existing fault signatures, including delta voltage or SOC, are not direct resistance health indicators (Zhou, Zheng, Pan, & Lu, 2021). Furthermore, the 12V battery in EVs is always in charging during vehicle power on or during external charger on. It's challenging to find a good excitation to estimate the resistance. In summary, there is a need to evaluate and develop more HIs suitable for EVs.

3. HEALTH INDICATOR DEVELOPMENT

The system flowchart for the proposed battery prognostics is shown in Figure 2 with following key steps: measuring battery signals, checking enabling conditions, estimating HIs, applying a decision-making algorithm, and notifying customers in case of a battery fault.

The battery voltage, current, SOC, and temperature are collected from onboard battery management system first. Subsequently, enabling conditions are applied to select data for robust health indicator generation. These conditions may include factors such as vehicle operational mode, temperature, or other signals. The details will be described later in this section.

Figure 2. The flowchart of 12V battery prognostics system.

Upon meeting the enabling conditions, the flowchart progresses to the calculation or determination of HIs based on the measured battery signal. These HIs offer valuable insights into the battery's performance. The vehicle operational modes correspond to varying phases where the battery experiences either charging or discharging processes:

1. **Power Off:** In this mode, the battery is inactive with negligible output current.
2. **Door Unlock/Exit:** This mode is usually brief, characterized by sensor activation to detect the vehicle owner's key. As such, the battery undergoes discharge.
3. **Accessory (Acc):** In this mode, the driver awakens the vehicle without putting it into motion. The battery continues to discharge.
4. **Driving:** This mode entails vehicle power on, initiating the operation of the high-voltage drive battery while the low-voltage battery is usually in a charging state.
5. **External Charging:** During this mode, the high-voltage battery is being charged externally, simultaneously recharging the low-voltage battery.

The driving profiles may be encountered in real-world driving scenarios, the charging and discharging states of the battery can be observed through the current-time curves. Battery charging or discharging state driving profile is shown in Figure 3, respectively. These identified modes allow us to tailor the development of candidates HIs based on the specific enabling conditions. The faults in LV batteries include internal short circuits or high internal resistance. The battery equivalent circuit diagram is shown as Figure 4.

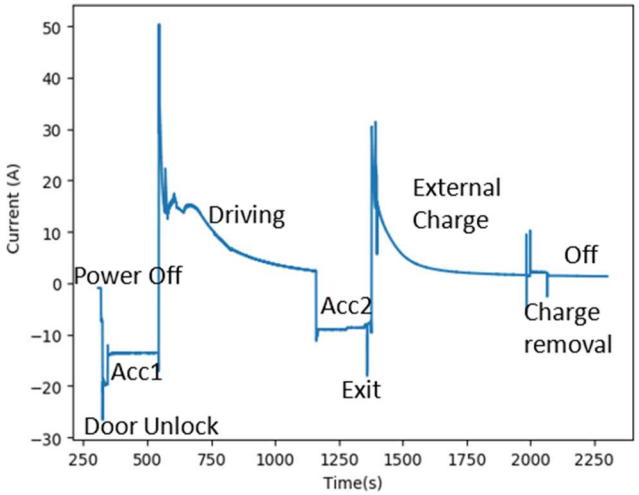

Figure 3. Battery charging/discharging state driving profile.

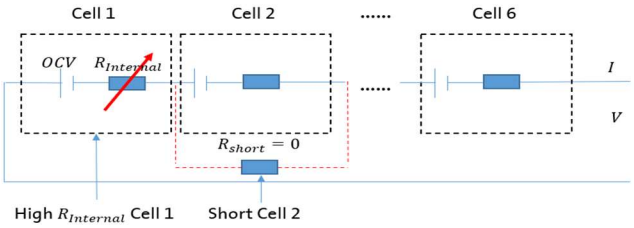

Figure 4. The equivalent circuit diagram for the 12V battery.

There are usually six identical cells connected in series inside the automotive LV battery. When the internal short circuit occurs, as illustrated for Cell 2 in Figure 4, the measured battery OCV will be reduced due to the fact that cell 2 is shorted. Therefore, it easy to detect internal short circuits through a measured decrease in OCV. The high internal resistance fault in Cell 1 is shown in Figure 4. When the internal resistance increases, the fault isolation is challenging because the internal resistance is typically in the milliohm level, and the resistance may not be accurately calculated under certain operation modes due to lack of enough excitation.

Considering the alternating charging and discharging states of batteries during operation, we developed HI candidates under different phases of charging and discharging. These indicators are specifically designed to accommodate various operational modes and effectively prognose the battery's health under different circumstances. The operating region of each HI is shown in Figure 5. The HI candidates include internal resistance during charge or discharge ($RhoC$, $RhoD$), internal resistance under charge-transition or discharge-transition phase (R_c, R_d) and corresponding OCV (OCV_c, OCV_d), ripple resistance (R_n), capacity deviation (dQ/dV), peak current and corresponding peak voltage ($Peak_I$, $Peak_V$).

3.1. Health Indicator Candidates

The first HI is the static resistance of the battery system during constant current charging or discharging, denoted as $RhoC$ or $RhoD$, respectively. Taking $RhoC$ as an example, the LV battery may be charged by Auxiliary Power Module (APM) during vehicle operations from the HV battery system and/or external charging system. In this work, $RhoC$ is estimated by Shepherd Equation (Mousavi G. & Nikdel, 2014), during vehicle driving when the LV battery is charged from the HV battery system,

$$RhoC = \frac{V_c - OCV}{I_c} \times \frac{C_n}{1 + \frac{M_c \times SOC}{C_c \times SOC}}, \quad (1)$$

where OCV is the open circuit voltage, SOC is the state of charge, V_c is the terminal voltage measured during constant charging, and I_c is the charging current. C_n is nominal capacity, M_c is a charge-transfer overvoltage coefficient, and

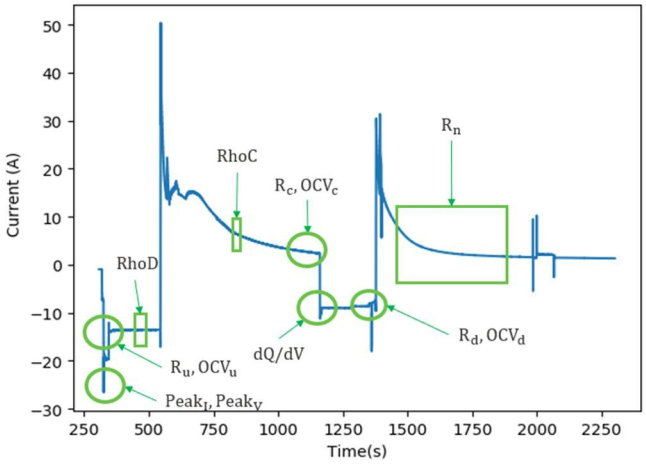

Figure 5. The operating region of each HI.

C_c is normalized capacity. The principles and calculations for $RhoD$ are analogous to those of $RhoC$, with the distinction that RhoD is computed specifically during discharge states, as shown in Figure 5. R_c, R_d, R_u, OCV_c, OCV_d, and OCV_u represent internal resistances and open-circuit voltage under different charging and discharging state. These parameters should be calculated when there is a variation in current. R_c and OCV_c are calculated when the battery is in the charging state. R_d, and OCV_d are calculated when the battery is in the discharging state. R_u, and OCV_u are calculated during vehicle door-unlock state while the battery is in the discharging state.

R_d and OCV_d are estimated by a 2P equivalent circuit model using the least squares method. The input data is the battery terminal current I, and the output is battery terminal voltage V. Using the least squares method, the 2P equivalent circuit model can be formulated as a linear equation as follows:

$$\boldsymbol{V} = \boldsymbol{X} * \boldsymbol{A}, \quad (2)$$

where the input $\boldsymbol{X}$ is a vector constructed from the current I, and the parameter vector $\boldsymbol{A}$ include R_d and OCV_d, which are expressed as following equations, respectively:

$$\boldsymbol{X} = [\boldsymbol{I}, 1], \quad (3)$$

$$\boldsymbol{A} = [R_d, OCV_d]^{\mathrm{T}}. \quad (4)$$

R_d, and OCV_d can then be estimated using the least square method as follows,

$$\boldsymbol{A} = (\boldsymbol{X}^{\mathrm{T}}\boldsymbol{X})^{-1}\boldsymbol{X}^{\mathrm{T}} * \boldsymbol{V}. \quad (5)$$

R_c and OCV_c, as well as R_u and OCV_u, can be calculated using a similar process as R_d and OCV_d. The difference lies in the battery's operational state during these measurements.

As we discussed above, the previous battery usage status along with the SOC level and charging or discharging current may impact the robustness of all resistance estimation. We will conduct a comparison based on the data to select the best health indicators for fault isolation.

In actual applications, the data are collected in real-time, and the algorithm will be executed under certain enabling conditions. The enabling condition is the key to improve the robustness of HIs. Taking R_d as an example, as shown in Figure 6, R_d and OCV_d are calculated when the battery is in the discharging state. The procedure commences by monitoring the power mode to ensure there is a sufficient duration of power-on (charging) before transitioning to the power-off mode. In this study, the power-on duration threshold is selected as 300s. Following this, the system initiates the recording of time, voltage, and current data upon the transition to power-off mode. The acquired data are funneled into a circular buffer with a predefined storage capacity. As the result, older data are automatically removed when new data are appended. It is noteworthy that, in this study, the buffer's capacity is limited to a 30-second duration. Once there are enough data in the buffer for resistance estimation, a subsequent verification is performed based on the current variation (*e.g.*, at least 8A). This step is crucial for confirming there is enough excitation for the data.

Nominal ripple resistance is denoted as R_n, which is the estimation of the battery resistance under small disturbances (ripples) during charging, namely R_p, and is then normalized by the temperature and the SOC using a look up table. A lower value of R_n corresponds to better battery health. The ripple resistance R_p is the ratio of the change in voltage to the change in current during charging, and is calculated based on the following equation:

$$R_p = \frac{V_{p1} - V_{p2}}{I_{p1} - I_{p2}} \tag{6}$$

where V_{p1} is measured voltage at a first sample time, V_{p2} is the measured voltage at a second sample time, I_{p1} is measured current at the first sample time and I_{p2} is the measured current at the second sample time. There always exist some ripples during charging, which is probably caused by poor filtering performance of the onboard chargers or other external disturbance. These ripples can provide enough excitation to make an effective estimation.

dQ/dV is another HI, which is the ratio of the change in electric charge Q, namely dQ, to the change in voltage, namely dV during discharging. dQ is calculated by coulomb counting, *i.e.* integrating the current samples over time, as illustrated in the following equation:

$$dQ = \int_{t1}^{t2} I(t)dt \tag{7}$$

$$\frac{dQ}{dV} = \frac{dQ}{V(t_2) - V(t_1)} \tag{8}$$

where $V(t_1)$ is the voltage at the timestamp t_1, and $V(t_2)$ is the voltage at the timestamp t_2. The dQ/dV values for good batteries are higher than those for faulty batteries. This is because healthy batteries can store more energy within the same voltage range.

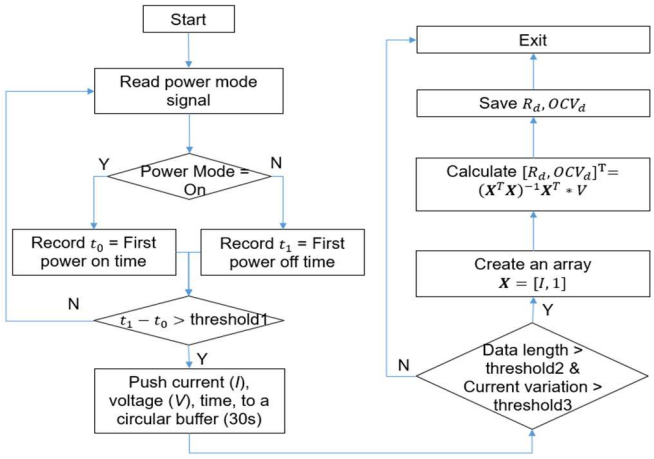

Figure 6. The flowchart for R_d calculation.

In this work, dQ/dV is calculated when the battery has just transitioned into a discharging state immediately after charging. Since the battery has just been charged, its voltage will decrease from 13V+ to about 12.5V due to both the relaxation process and the discharge current impact. When using the dQ/dV method to evaluate battery performance, it is essential to ensure that the battery voltage change is equal to a predefined value. This consistency ensures that dV values are identical across measurements. By maintaining the same voltage range, we can accurately evaluate the influence of dQ variations and reliably assess the battery's performance. It's challenging to estimate dQ/dV under charging, because due to different driving habits and charging habits, it is difficult to find areas that cover the same voltage. However, it's more common to identify a voltage range of 12.7V to 12.9V after charging since the battery charging voltage is normally above 13V. Calculating dQ/dV can be done in a short amount of time, and the working conditions are relatively stable, making dQ/dV an effective indicator for diagnosis.

The flowchart for dQ/dV calculation is shown as Figure 7. The initial phase closely mirrors the R_n calculation process, wherein it is important that the battery has undergone a sufficient charging duration. This recorded data is subsequently stored in a buffer capable of retaining information for up to 120 seconds. The subsequent step involves the selection of continuous data points displaying voltage variations within a predefined range. In this research, data points lying within the voltage range of 12.7V to 12.9V are specifically chosen. Coulomb counting is then applied to precisely quantify the charge discharged from the battery throughout this interval. Ultimately, the dQ/dV value is computed employing the dQ/dV formula (Eq. 8) to provide

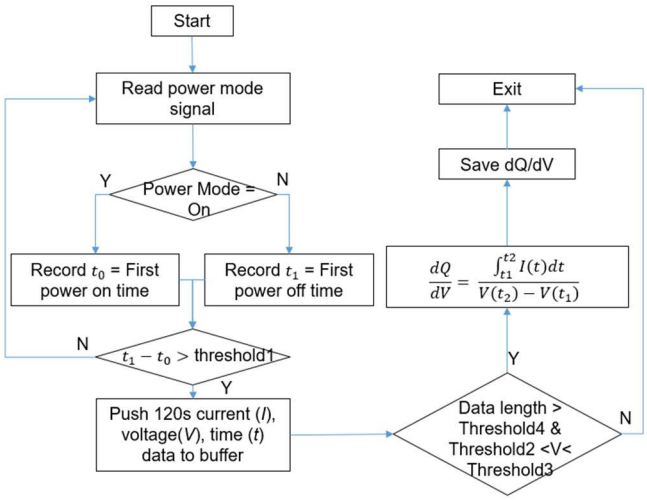

Figure 7. The flowchart of dQ/dV calculation.

a comprehensive assessment of the battery's electrochemical behavior. The discharge current during certain transient events, such as opening car doors, turning on vehicle lights, or activating in-car media systems, can be relatively high due to the load. The peak current Peak_I and the peak voltage Peak_V during these transient events can provide insights into the battery's health condition.

3.2. Health Indicator Selection

The developed candidate HIs encompass both charging and discharging states. However, the performance of each HI in fault prognostics may vary due to different noise factors. Only the HIs with high performance should be selected.

We first evaluate the effectiveness of HIs based on theoretical analysis. As we known, LV batteries, mainly lead-acid batteries, are strongly impacted by the previous usage status. For example, sulphation or sulfate-crystal formation increases the internal resistance (Lam, et al., 1995), which may occur after several days of inactivity or may be reduced with certain charging current. Since $RhoD$, R_u, $Peak_I$, and $Peak_V$ are estimated right after the start, but $RhoC$ and R_c, R_d, R_n, and dQ/dV are estimated after several minutes of discharging and charging, former HIs may be impacted more by the previous usage and consequently might be less robust. R_d is normally more reliable than R_c. There are two scenarios for R_c calculation. (1) if R_c is calculated during charging, the voltage variation and the current variation are mainly caused by the OCV increase and the charge efficiency decrease, which leads to insufficient excitation for resistance estimation. (2) if R_c is calculated using the data from the end of charging to discharging, the voltage variation is heavily impacted by the hysteresis and polarization process, but not ohmic resistance. OCV and internal resistance are estimated simultaneously. OCV is mainly impacted by SOC, which may not help to isolate low capacity or high resistance. Hence, it is anticipated that indicators $RhoC$, R_d, R_n, and dQ/dV would exhibit better performance in battery prognostic.

The data-driven method is also employed to evaluate and select HIs in this work. Here the performance of different HIs is compared by using metrics such as precision, recall, F1 score, and ROC/AUC (Mu, Liu, Ewing, & Li, 2021). The formulas for precision, recall, and F1 score are shown as follows:

$$Precision = \frac{TP}{TP + FP} \tag{9}$$

$$Recall = \frac{TP}{TP + FN} \tag{10}$$

$$F1\ Score = 2 * \frac{Precision * Recall}{Precision + Recall} \tag{11}$$

Precision indicates how precise the prediction "Faulty" is. Recall measures the percentage of actual faulty batteries that are correctly classified. F1 score is the harmonic mean of recall and precision. An ROC curve illustrates the balance between true positive rate and false positive rate at various threshold levels. The curve closer to the upper left corner indicates better HI performance. AUC is the area under the ROC curve, which is a metric used to quantify the performance of ROC curve. The performance metrics of each HI are discussed in Section 4. Eventually, $RhoC$, R_d, R_n, and dQ/dV were selected based on both theoretical analysis and data-driven evaluation.

4. EXPERIMENT AND RESULT

The developed HIs along with the detailed calculation process are discussed in the Section 3. Experiment design and the HIs performance will be shown in this section.

4.1. Experiment Design

The experiments are conducted on a GM test EV. Two batteries are prepared for the experiments: one is a healthy battery, and the other is a faulty battery. The faulty battery is a warranty returned part and classified as "high resistance battery" by the battery tester. Even though the performance of this battery is degraded, it can still be used to start the vehicle. Data collection is performed per driving profiles, whose details are listed in Table 1.

Driving profile encompasses nine different modes, spanning the entire process from the driver getting ready to drive, through driving, charging, and power off. In each of these modes, the battery may be either in a charging or discharging state. These states are the most common states in the field.

The collected data include the current, the voltage, the time, and the temperature. The sampling rate is 10 ms/sample. In the experiments, the influence of the initial SOC levels and the temperature on the battery is also investigated. Since the vehicle battery might be at different SOC before starting,

Table 1. Driving profile.

Step	Mode description	Time	Battery State
1	Power Off	2 mins	No charging or discharging (Current = 0)
2	Door Unlock / Enter vehicle	0.5 mins	Battery discharging (Current < 0)
3	Accessory 1 (No brake, press and hold power button 5 seconds,)	3 mins	battery discharging (Current < 0)
4	Start vehicle (brake pedal, push and release power button, but no driving)	10 mins	Battery charging (Current > 0)
5	Accessory 2 (Push and release Power button again)	3 mins	Battery discharging (Current < 0)
6	Exit vehicle (Open and close door)	0.5 mins	Battery discharging (Current <0)
7	External charging (Charger plug in)	10 mins	Battery charging (Current > 0)
8	External Charging removes	5 mins	Battery discharging (Current <0)
9	Off	5 mins	No charging or discharging (Current = 0)

experiments are conducted with the initial battery SOC around 30%, 60%, and 85%, respectively.

Temperature is a critical factor affecting battery performance, especially in cold weather, where it might increase battery internal resistance. Our experiments are conducted at 0 ℃ and 25 ℃, respectively.

4.2. Health Indicators Performance

With the experiment described in 4.1 (one test vehicle and two batteries), the performance for various HIs is presented using the boxplot graphs and the evaluation metrics described in Section 3.2 to illustrate the fault isolation capability of different HIs. We use Python 3.9, NumPy 1.23.4 and Pandas 1.5.1 package to process all the data. All the tests are conducted on a windows computer with Intel I5-8365 CPU and 16G memory.

All the boxplot graphs have two columns. The left column represents the healthy battery, and the right column represents the faulty battery with high resistance. Each boxplot presents one HI calculated at different initial SOC levels (30%, 60%, 85%) under the same temperature (25℃). The HI performance for low temperature (0℃) will be discussed later. The boxplots provide an overview of the distribution of HI values, which are normalized to 0-1 enabling the comparison between good and faulty batteries. This information can be used to establish thresholds for diagnosis. All normalized HIs' boxplots are shown in Figure 8 and Figure 9.

The evaluation metrics of the HIs under 25℃ are shown in Table 2. Low precision indicates that a number of samples have been incorrectly classified as faulty battery samples, when they are actually healthy battery samples. Low recall means that a number of faulty battery samples are missed or not detected by this HI. The selected good HIs include $RhoC$, R_d, R_n and dQ/dV, which is with at least 0.80 for F1 score, AUC value, precision, and recall.

In Figure 8, $RhoC$, R_d, R_n and dQ/dV can effectively distinguish healthy and faulty batteries as shown by the boxplots, whereas the results for $RhoD$ and R_c exhibit significant overlap in their distributions. It's evident that, for HIs related to resistance such as $RhoC$, R_d, and R_n, the values for the faulty battery are generally higher than those for good batteries. This result confirms the fact that the faulty battery indeed exhibits higher resistance. For dQ/dV, the values for the good battery are higher than those for the faulty battery. These results align with the physical insight we considered during the development of HIs.

The robustness of the selected HIs is evaluated to ensure their effectiveness with different noise factors. To investigate the impact of temperature, data is collected for both 0 ℃ and 25 ℃. The results are shown in Figure 9.

In Figure 9, and Table 3, one can observe that at low temperatures, although the performance of RhoC becomes slightly worse compared to that under 25 ℃ only, $RhoC$, R_d, R_n and dQ/dV can still effectively differentiate healthy and faulty batteries. This result indicates that the performance of $RhoC$, R_d, R_n and dQ/dV can be used to diagnose most faulty batteries when the ambient temperature is under 0 ℃ and 25 ℃. Since R_n is already normalized by the temperature and dQ/dV is not resistance-based feature, their robustness is the best among all HIs. Further temperature compensation

Table 2. Performance of all HI at 25℃.

HIs	F1 score	AUC	Precision	Recall
$\boldsymbol{RhoC}$	0.8749	0.95	0.8125	0.9285
$RhoD$	0.4666	0.41	0.0625	0.5000
R_c	0.7500	0.50	0.5000	0.7500
$\boldsymbol{R_d}$	0.8333	0.96	0.8125	0.9285
R_u	0.6521	0.50	0.0625	0.5000
$\boldsymbol{R_n}$	0.9655	1.00	1.0000	0.9444
$\boldsymbol{dQ/dV}$	0.9230	0.98	0.8823	1.0000
ocv_d	0.6428	0.50	0.1000	0.5000
ocv_u	0.6530	0.50	0.0588	0.5000
$Peak_I$	0.6521	0.57	0.0588	1.0000
$Peak_V$	0.6250	0.63	0.5882	0.6666

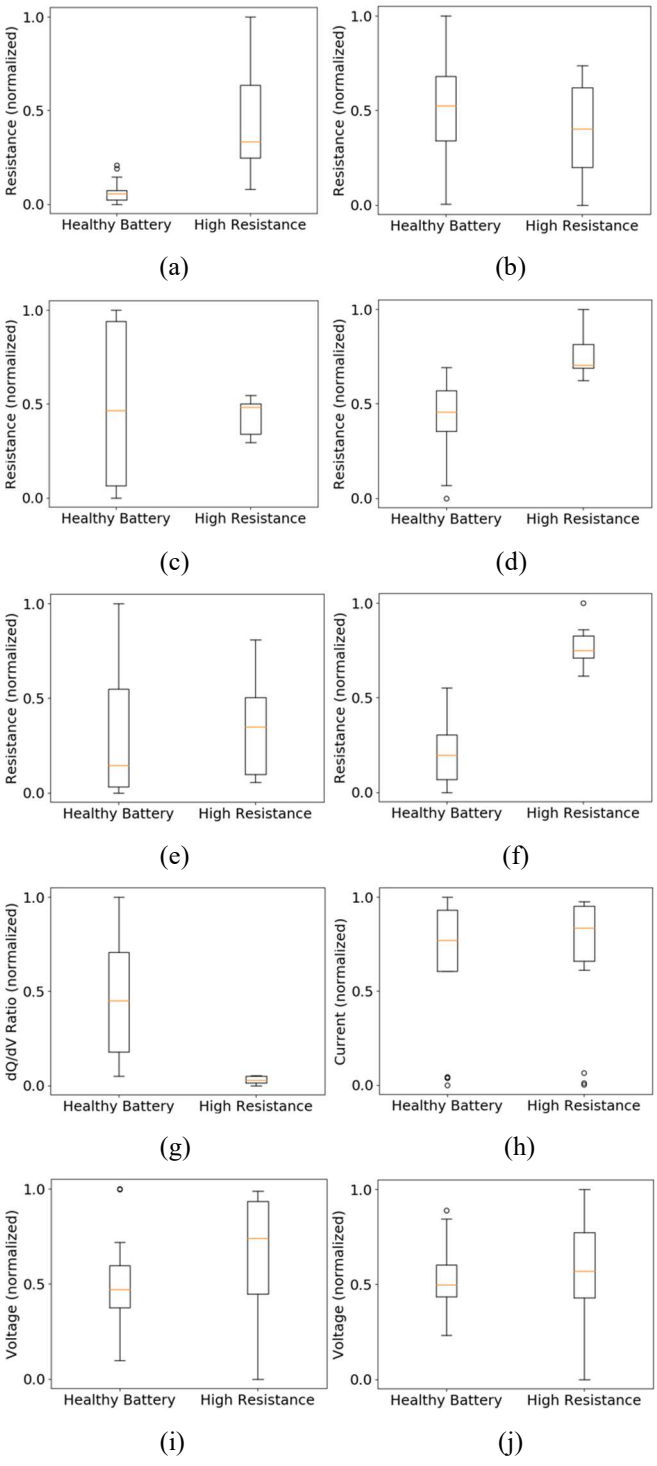

Figure 8. The performance of each normalized HI: (a) $RhoC$, (b) $RhoD$, (c) R_c, (d)R_d, (e)R_u, (f)R_n, (g) dQ/dV, (h) Peak Current ($Peak_I$), (i) Peak Voltage ($Peak_V$), and (j) OCV_d.

on these HIs may further mitigate the influence of the temperature, allowing for more precise and consistent predictions. The data sampling rate of the onboard system is 10 ms/sample, while the offboard system typically has a much lower sampling rate, such as 200 ms/sample. Since $RhoC$ can be estimated from one timestamp data, differences in sampling rates do not affect the results. Since R_n is an onboard calculation from IBS (intelligent battery sensor), the sampling rate during estimation can't be changed. To test our algorithm's performance for R_d and dQ/dV, we down sampled the data to 200 ms/sample. The performance of R_d and dQ/dV is summarized in Table 4. The normalized dQ/dV ratio boxplot is selected as an example, as shown in Figure 10.

It appears that calculating HIs with the down-sampled data had little impact on their performance, and the results remain consistent with those obtained at a 10ms/sample sampling rate. This suggests that the developed HIs can adapt to low-sampling-rate conditions effectively.

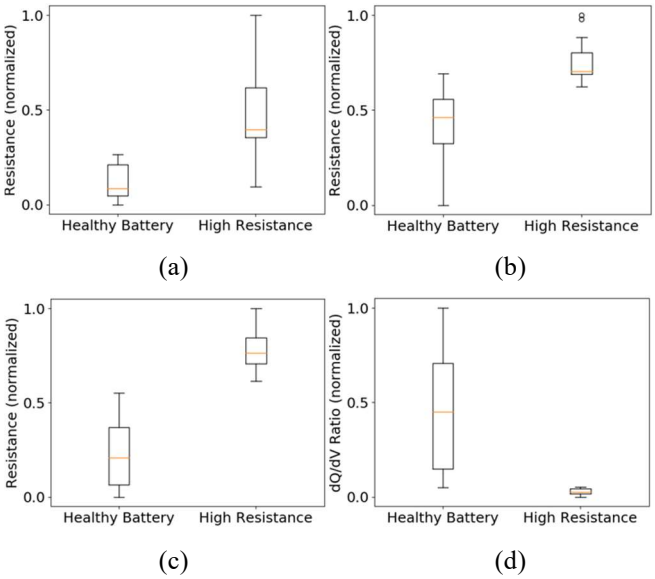

Figure 9. The normalized HI performance at 0℃ and 25 ℃: (a) $RhoC$, (b) R_d, (c) R_n, and (d) dQ/dV.

Table 3. The HIs performance at 0℃ and 25 ℃

HIs	F1 score	AUC	Precision	Recall
$RhoC$	0.8717	0.94	0.9523	0.8333
R_d	0.8571	0.96	0.8095	0.9444
R_n	0.9756	1.00	1.0000	0.9583
dQ/dV	0.9444	0.99	0.9000	1.0000

Table 4. The HI performance for data with the sampling rate of 200 ms/sample.

HIs for 200 ms/sample	F1 score	AUC	Precision	Recall
R_d	0.8571	0.91	0.9230	0.9230
dQ/dV	0.9090	0.97	0.8333	1.000

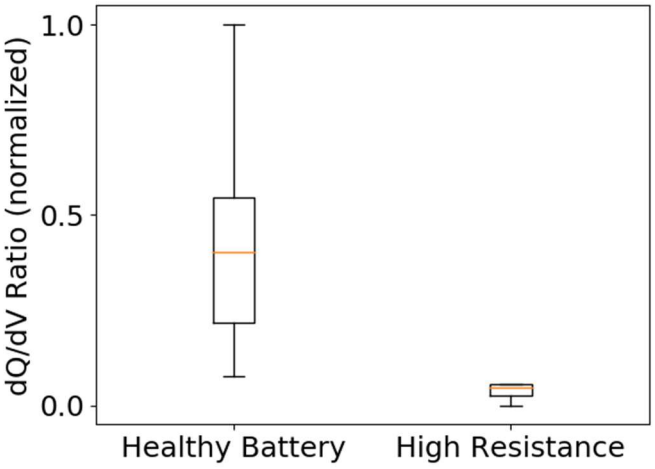

Figure 10. The normalized dQ/dV results from data with the sampling rate of 200 ms/sample.

5. CONCLUSION

A novel diagnostic and prognostic solution of low-voltage batteries for electric vehicles is developed. The proposed solution does not necessitate additional sensors for capturing new signals. Instead, it utilizes the existing signals, including current, voltage, state of charge, and temperature to generate 4 health indicators (HIs), which are able to predict battery failures accurately and robustly in diverse driving scenarios and under wide temperature variations. The key takeaways are summarized as follows: (1) Internal resistance during charging, internal resistance from discharging to charging transition, normalized ripple resistance and dQ/dV during ignition off along with corresponding enabling conditions are selected as effective HIs, whose F1 scores are 0.87, 0.83, 0.96, 0.92, respectively. (2) Internal resistance during discharging, internal resistance from charging to discharging transition, open circuit voltage (OCV), peak current ($Peak_I$), peak voltage ($Peak_V$), and dQ/dV under various driving modes are identified as ineffective HIs. (3) The selected HIs show robust performance against the temperature or SOC variations. The F1 score is more than 0.85 under different scenarios.

Even though the algorithm has been validated on a real vehicle, a large-scale test on several thousand vehicles with more than 1 year data is still required to ensure the desired performance in terms of false positive rate and false negative rate. The impact of other noise factors *e.g.* various failure modes will be investigated as well. In terms of SOH prognostics or remaining useful life estimation, a large amount of ageing data will be collected, and the prognostic model will be developed in the future. Future development work may also be focused on low voltage batteries with other chemistry *i.e.*, Li-ion or other new low voltage power sources.

REFERENCES

Cheng, S., Azarian, M., & Pecht, M. (2010). Sensor Systems for Prognostics and Health Management. *Sensors, 10*(1424-8220), 5774-5797.

Du, X., & Zhang, Y. (2018). Development of Robust Fault Signatures for Battery and Starter Failure Prognosis. *Annual Conference of the PHM Society. Vol. 10. No. 1.*

Emadi, A., Williamson, S. S., & A. Khaligh. (2006). Power electronics intensive solutions for advanced electric hybrid electric and fuel cell vehicular power systems. *IEEE Trans. Power Electron., 21*(3), 567-577.

G., S. M., & Nikdel, M. (2014). Various battery models for various simulation studies and applications. *Renewable and Sustainable Energy Reviews, 32*(1364-0321), 477-485.

Hasan, M. K., Mahmud, M., Habib, A. A., Motakabber, S., & Islam, S. (2021). Review of electric vehicle energy storage and management system: Standards, issues, and challenges. *Journal of Energy Storag, 41*, 102940.

Hou, R., Magne, P., Bilgin, B., & Emadi, A. (2015). A topological evaluation of isolated DC/DC converters for auxiliary power modules in electrified vehicle applications. *Proc. IEEE Appl. Power Electron.Conf.* . Expo.

Khan, S., & T. Yairi. (2018). A review on the application of deep learning in system health management. *Mechanical Systems and Signal Processing, 107*, 241-265.

Lam, L., Ozgun, H., Lim, O., Hamilton, J., Vu, L., Vella, D., & Rand, D. (1995). Pulsed-current charging of lead/acid batteries - a possible means for overcoming premature capacity loss. *Journal of Power Sources*, 215-228.

Mu, H., Liu, J., Ewing, R., & Li, J. (2021). Human Indoor Positioning via Passive Spectrum Monitoring. *2021 55th Annual Conference on Information Sciences and Systems (CISS)*, (pp. 1-6). Baltimore, MD.

Naha, A., Khandelwal, A., Agarwal, S., Tagade, P., Hariharan, K. S., Kaushik, A., . . . Oh, B. (2020). Internal short circuit detection in Li-ion batteries using supervised machine learning. *Scientific Reports, 10*(1), 1301.

Ng, S. S., Xing, Y., & Tsui, K. L. (2014). A naive Bayes model for robust remaining useful life prediction of lithium-ion battery. *Applied Energy, 118*(0306-2619), 114-123.

Olabi, A., Abdelghafar, A. A., Soudan, B., Alami, A. H., Semeraro, C., Radi, M. A., . . . Abdelkareem, M. A. (2024). Artificial neural network driven prognosis and estimation of Lithium-Ion battery

states: Current insights and future perspectives. *Ain Shams Engineering Journal, 15*(2), 102429.

Samanta, A., Chowdhuri, S., & Williamson, S. (2021). Machine Learning-Based Data-Driven Fault Detection/Diagnosis of Lithium-Ion Battery: A Critical Review. *Electronics , 10*, 1309.

Wang, C., Zheng, P., & J. Bauman. (2023). A Review of Electric Vehicle Auxiliary Power Modules: Challenges, Topologies, and Future Trends. *IEEE Transactions on Power Electronics, 38*(9), 11233-11244.

Xing, Y., Ma, E. W., Tsui, K.-L., & Pecht, M. (2013). An ensemble model for predicting the remaining useful performance of lithium-ion batteries. *Microelectronics Reliability, 53*(6), 811-820.

Zhao, G., Zhang, G., & Ge, Q. (2016). Research Advances in Fault Diagnosis and Prognostic Based on Deep Learning. *IEEE Prognostics and System Health Management Conference.* Chengdu, China.

Zhou, W., Zheng, Y., Pan, Z., & Lu, Q. (2021). Review on the Battery Model and SOC Estimation Method. *Processes, 9*, 1685.

ACKNOWLEDGEMENT

The authors would like to thank Yilu Zhang and Sanjeev Naik for their support of this research.

BIOGRAPHIES

Xinyu Du received B.Sc. and M.Sc. degrees in automation from Tsinghua University, Beijing, China, in 2001 and 2004, respectively, and a Ph.D. in electrical engineering from Wayne State University, MI, USA, in 2012. He has been working at General Motors Global R&D Center, Warren, MI, since 2010, and currently holds the staff researcher position in the vehicle systems research lab. He has published more than 50 peer review papers and holds 99 patents or patent applications. He has been serving as an associate editor for 4 internal journals. He received two best conference paper awards, in 2019 and 2020, respectively, and two Boss Kettering Awards from General Motors for his contribution in vehicle health management.

Huaizheng Mu received the B.Sc. in optoelectronic information science and engineering from the Beijing Information Science and Technology University, Beijing, China, in 2018, and the M.Sc. in electrical and computer engineering from Oakland University, Rochester, MI, USA, in 2021. He joined General Motors R&D, Warren, MI, in 2022 and currently is a researcher in the Propulsion Systems Research Lab. His research interests include signal processing, deep learning, vehicle health management, and failure diagnosis & prognosis of various vehicle systems.

Kevin Corr received his BSE (E.E.) from The University of Michigan in 2003. He has worked on Low Voltage Battery Prognostics at General Motors since 2016. He previously worked on a Vehicle Health Management System for the Gun-Turret Drive on Abrams tanks at General Dynamics Land Systems.

Matt Nowak received a BE from Dartmouth College in Hanover, NH in 2002. He has been working at the General Motors Technical Center, Warren, MI since 2017 and currently holds a senior data engineer position in the Electrical and Thermal Prognostics team. His focus is around 12V battery systems. He holds 5 patents related to controls software for automatic transmissions.

Hong Wong currently holds the engineering group manager position in the Electrical and Thermal Prognostics team.

Tung-Wah Frederick Chang currently holds a senior data engineer position in the Electrical and Thermal Prognostics team.

Sara Rahimifard received her Ph.D. in Mechanical Engineering from McMaster University, Canada, in 2022, M.Sc. degree in electrical engineering from Amirkabir University of Technology, and B.Sc. degree in electrical engineering from Shiraz University, Iran. She has been working at General Motors, Canadian Technical Center, Markham, ON, since 2022, where she develops prognostics algorithms for electric vehicles.